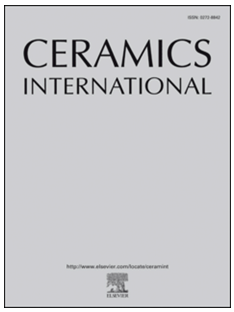

Enhanced strength and thermal oxidation resistance of shaddock peel-polycarbosilane-derived C–SiC–SiO_2 composites

Guo-Qing Li, Min Yu, Guo-Wei Lin, Yun-Long Wang, Li-Xia Yang, Ji-Xuan Liu, Francesco Gucci, Guo-Jun Zhang

PII: S0272-8842(22)02037-5

DOI: https://doi.org/10.1016/j.ceramint.2022.06.045

Reference: CERI 33053

To appear in: *Ceramics International*

Received Date: 28 March 2022

Revised Date: 23 May 2022

Accepted Date: 4 June 2022

Please cite this article as: G.-Q. Li, M. Yu, G.-W. Lin, Y.-L. Wang, L.-X. Yang, J.-X. Liu, F. Gucci, G.-J. Zhang, Enhanced strength and thermal oxidation resistance of shaddock peel-polycarbosilane-derived C–SiC–SiO_2 composites, *Ceramics International* (2022), doi: https://doi.org/10.1016/j.ceramint.2022.06.045.

Ceramics International, Volume 48, Issue 19, Part A, October 2022, pp. 27516-27526
DOI: 10.1016/j.ceramint.2022.06.045

Enhanced strength and thermal oxidation resistance of shaddock peel-polycarbosilane-derived C-SiC-SiO_2 composites

Guo-Qing Li [1], Min Yu [1,*], Guo-Wei Lin [2], Yun-Long Wang [1], Li-Xia Yang [1], Ji-Xuan Liu [2], Francesco Gucci [3], Guo-Jun Zhang [2]

[1] College of Materials Science and Technology, Nanjing University of Aeronautics and Astronautics, Nanjing 211106, China

[2] State Key Laboratory for Modification of Chemical Fibers and Polymer Materials, Institute of Functional Materials, College of Materials Science and Engineering, Donghua University, Shanghai 201620, China

[3] Surface Engineering and Precision Institute, Cranfield University, Bedfordshire MK430AL, UK

Abstract: Biomorphic ceramic materials have potential high-temperature applications, owing to their low density, good corrosion resistance and excellent shape capability, but achieving both high specific strength and excellent thermal oxidation resistance is challenging. In this report, shaddock peel-derived C-SiC-SiO_2 composites were successfully prepared by the polymer precursor infiltration (PPI) technique with an optimized heating program. The composites prepared at 1600 ℃ exhibit the highest compressive strength (~ 14.0 MPa) and specific strength (~ 1.5×10^7 N·m/kg), while those sintered at 1200 ℃ exhibit the highest bending strength (~ 27.4 MPa). The composites exhibit good thermal oxidation resistance (up to 1400 ℃) with a low weight loss ratio (<0.11 g/cm^3), moreover, the compressive strength of the composites sintered at 1200 ℃ after thermal oxidation at 1400 ℃ surprisingly increased from 11.6 ± 2.7

* Corresponding author: Min Yu
College of Materials Science and Technology,
Nanjing University of Aeronautics and Astronautics, Nanjing 211106, China
E-mail: min.yu@nuaa.edu.cn

MPa to 21.5 ± 3.5 MPa. The PPI technique provides a viable route to introduce Si source into natural materials and the shaddock peel-derived C-SiC-SiO_2 composites are light materials with high strength and excellent high-temperature thermal oxidation resistance.

Keywords: shaddock peel, polycarbosilane, composites, strength, high-temperature oxidation resistance

1. Introduction

Recently, a new class of biomorphic ceramics have attracted a lot of attention in structural design to produce biomorphic ceramic composites [1-3]. Natural materials-derived structural ceramics have potential high-temperature applications (i.e. aerospace materials, heat storage materials, high-temperature gas/liquid filters etc.), owing to their high-temperature oxidation resistance, low density, excellent corrosion resistance and complex shape capability [1, 4, 5]. A lot of natural materials have been explored for producing structural ceramics, such as pine [6], oak [7], birch [8], iroko [9], bamboo [10], beech [11], balsa [12], sipomahogany [13] and coir fiberboard [14]. However, the cellular pore structures of these natural materials significantly restrict the infiltration of a second material to produce a biomorphic ceramic with uniform microstructure and high strength. Exploring natural materials with interconnected pore structures could potentially improve the infiltration efficiency and produce biomorphic ceramics with high strength. Shaddock peel, for example, has a three-dimensional interconnected pore structure (pore size: 300 ~ 500 μm, porosity: ~ 85%), which would be beneficial to infiltrate another material into the original structure. Most research focus on infiltrating the second materials into carbonized wood (bulk or powder biochar), leading to extra pyrolysis process before infiltration and the separation between slurry and template [6, 7, 15-17]. It would be beneficial to infiltrate the second material directly into uncarbonized wood, in order to shorten process and avoid macro-cracks. Another benefit of using a material like shaddock peel is the fact that it could be easily shaped into relatively complex shapes before the infiltration and is a cheap waste substrate.

The objective of this work is to obtain a shaddock peel-derived ceramic composites with both high specific strength and high-temperature (up to 1400 ℃) thermal oxidation resistance. The introduction of a Si source in the shaddock peel offers the possibility to obtain a porous SiC ceramic during the high-temperature heat treatment in an inert atmosphere. Several infiltration techniques have been developed for producing biomorphic SiC ceramics derived from natural materials, including chemical vapor infiltration (CVI), melt infiltration (MI), sol-gel infiltration (Sol-gel), slurry infiltration (SI), polymer precursor infiltration (PPI) and molten salt infiltration (MSI) [1, 5, 9, 10, 18-21]. The mechanical properties of wood-derived biomorphic SiC prepared only by MI were reported, while the comprehensive mechanical properties of those produced by CVI, Sol-gel and SI were barely reported, probably owing to their inhomogeneous microstructures. Compared with the methods above, the polymer precursor infiltration (PPI) technique has some advantages such as low sintering temperature, simple production process and the ability to completely retain the original structure of natural materials [15, 22, 23]. The production of wood-derived SiC ceramics usually requires more than 5 repeated infiltration steps which can last for 9 hours per each step [11]. However, the use of shaddock peel as template could reduce the number of infiltrations and shorten the whole processing time.

Another additional problem arising in the production of wood-derived ceramics, is the formation of macro-cracks due to the rapid change of water content during the heating process, which negatively affect the mechanical properties of ceramics [24, 25]. The heating profile significantly affects the microstructure and mechanical properties of the polycarbosilane (PCS)-derived SiC in the SiC_f/SiC composites but limited amount of research was found investigating the effect of heating profiles on the microstructures of biomorphic ceramics [26, 27].

Wood has good room-temperature mechanical properties with the compressive strength reaching up to ~ 47 MPa and bending strength reaching up to ~ 79 MPa, while the wood-derived C-SiC composites were reported to have compressive strength of ~ 12 MPa in the radial direction and ~ 25 MPa in the axial direction, and bending strength

of 16 ~ 42 MPa [13, 24, 28, 29]. Few research about the high-temperature oxidation resistance of biomorphic ceramics has been reported.

In this work, shaddock peel-derived biomorphic C-SiC-SiO_2 composites were produced by polymer precursor infiltration and sintered under a general heating program and an optimized heating program. Effects of each infiltration cycle and heating program on the microstructures of the biomorphic composites were investigated thoroughly. The compressive strength, bending strength and thermal oxidation resistance (500 ~ 1400 ℃) of the biomorphic C-SiC-SiO_2 composites were evaluated in details. The compressive strength and bending strength of the biomorphic C-SiC-SiO_2 composites after oxidation at 1400 ℃ were also evaluated, for the first time. More importantly, the strengthening mechanisms of the self-healing during the thermal oxidation at 1400 ℃ were proposed and further confirmed by SEM.

2. Experimental procedure

2.1 Material preparation

Shaddock peel (from Meizhou, Guangdong, China) was dried at 80 ℃ for 24h, and the polycarbosilane (PCS)-xylene solution was prepared by mixing polycarbosilane with molecular weight between 1200 and 1500 (China Fujianliya Xin Material Co., LTD.) and xylene (Shanghai Maclin Bio-chemical Technology Co., LTD.) with a mass ratio of 1:2 at room temperature. The dried shaddock peel was placed in the prepared polycarbosilane (PCS)-xylene solution and vacuum-infiltrated for 5 mins. The infiltrated samples were taken out and dried for 10h in an oven at 120 ℃ to fully remove the residual xylene solvent. The vacuum infiltration-drying process was repeated for 3 times to ensure efficient infiltration of PCS. The mass of the infiltrated samples was measured after each infiltration cycle. Finally, the shaddock peel/PCS composites were sintered in an Ar-rich atmosphere (99.1% Ar + 0.9% O_2) under the general heating program-1 and the optimized heating program-2 (as shown in the insets in Fig. 3b and c) to obtain the biomorphic C-SiC-SiO_2 composites derived from shaddock peel. Fig. 1a shows the whole preparation process of the shaddock peel-derived C-SiC-SiO_2 composites. Fig. 1b shows the physical dimension of the samples. Finally, C-SiC-SiO_2

composites were oxidized at 500 ~ 1400 ℃ for 45 mins and characterized.

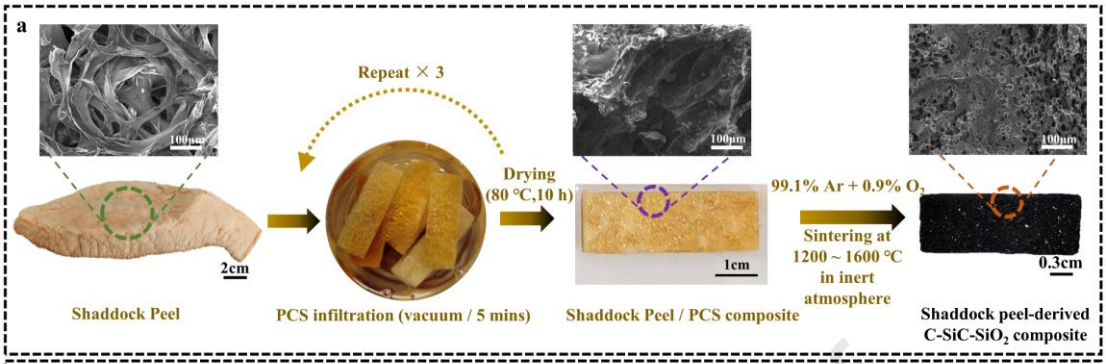

b

The physical dimension of the samples (length × width × height)		
	Bending test	Compression test
Shaddock peel (mm)	35.0 × 14.0 × 8.0	20.0 × 20.0 × 9.0
Shaddock peel / PCS (mm) (polished)	33.0 × 13.6 × 7.8	18.0 × 18.0 × 8.0
C-SiC-SiO_2 composites (mm) (polished)	23.0 × 10.5 × 6.0	10.0 × 10.0 × 5.0

Note : The physical dimension of the samples in the table are the physical dimension of the samples that has been polished.

Fig. 1(a) Preparation process of the biomorphic C-SiC-SiO_2 composites derived from shaddock peel. (b) the physical dimension of the samples.

2.2 Characterization

Thermogravimetric analysis (TGA) was used to determine the weight loss during the heat treatment (from 100 ℃ to 1000 ℃) with a heating rate of 5 ℃/min in flowing N_2. The microstructure of the samples was investigated by inspect-F scanning electron microscope (SEM, Hillsboro, OR). X-ray diffraction (XRD) analysis was used to detect the phases in the samples using Cu Kα radiation (Malvern Panalytical-Empyrean ALPHA1, England). The computed tomography scanner (CT, YXLON FF35) was used to investigate the tomography of the composites. Intelligent oxygen analyzer (Hangzhou Jiachang Electronic Technology Co., LTD., China) was used to test the oxygen content in the atmosphere of the furnace. Universal testing machine (Jinan metus testing technology-CMT5000 Co., LTD., China) was used to test the mechanical properties of C-SiC-SiO_2 composites, including three-point bending test (span: 16 mm; the radius of header and base: 5 mm, 23 mm × 10.5 mm × 6 mm), compression test (10 mm × 10 mm × 5 mm), and anti-oxidation performance test (10 mm × 10 mm × 5 mm).

3. Results and discussions

3.1 Effect of infiltration times on the weight gain rate of composites

Fig. 2a-d show the microstructures of the shaddock peel after different infiltration-drying cycles. The shaddock peel exhibits uniform, nearly hexagonal and reticular macropores, as shown in Fig. 2a. The shaddock peel presents a natural three-dimensional interconnected pore structure that allows the following PCS to quickly and evenly infiltrate into the peel. It takes 9h for each infiltration and at least 5 infiltrations to prepare the biomorphic pine-derived ceramic by sol-gel infiltration [30], while it takes only 5 mins for each infiltration and infiltrations to prepare the shaddock peel-derived ceramic by polymer precursor infiltration.

As shown in Fig. 2b, PCS was uniformly and continuously attached to the shaddock peel. Fig. 2c exhibits more PCS attached to the shaddock peel after the second infiltration, while it fully filled the shaddock peel after the third infiltration, as shown in Fig. 2d. The PCS can be easily attached to the shaddock peel, owing to the hydrogen bonds of PCS and between PCS (-Si-H) and cellulose (-O-H), while it was difficult to infiltrate PCS into the carbonized shaddock peel (as shown in supplementary Fig. S1), probably because PCS has higher wettability on shaddock peel, instead of carbon [31].

An indicator of the infiltration efficiency is the weight gain rate (WGR, wt.%) after infiltration in Fig. 2e. The weight gain rate for each cycle is calculated using the following Eq. (1).

$$WGR = \frac{w_b - w_a}{w_a} \times 100\% \quad (1)$$

Where w_a: weight of the shaddock peel before infiltration (g); w_b: weight of shaddock peel after infiltration (g). Each shaddock peel has the same length, width and height.

As shown in Fig. 2e, the highest weight gain rate of shaddock peel after single infiltration-drying cycle is 252.4 wt.%, and the total weight gain rate of shaddock peel after three infiltration-drying cycles is 540.9 wt.%. The weight gain of pine derived carbon template after the third infiltration of SiO_2 gel was only 77 wt.%, which was not enough to fully convert carbon to SiC [32]. However, the weight gain rate of the dried

shaddock peel is up to 540.9%, indicating that PCS was efficiently infiltrated into the shaddock peel to form SiC by polymer precursor infiltration.

Fig. 2f shows that the shaddock peel has the highest weight gain rate of 540.9 wt.%, compared with pine, oak, ayous and iroko (338.0 ~ 166.7 wt.%) [28, 29, 33], thus PCS-xylene solution can be easily infiltrated into the shaddock peel.

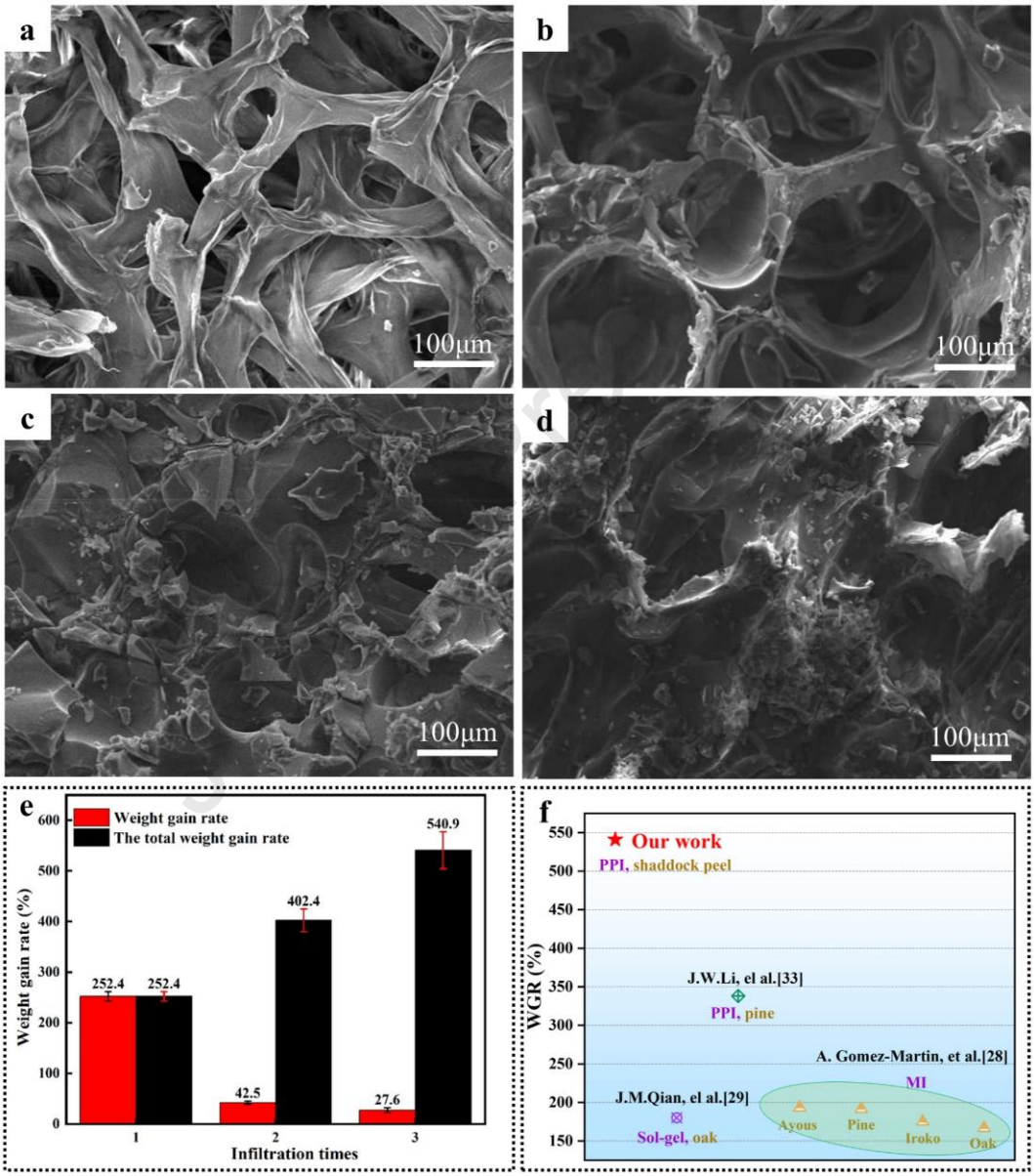

Fig. 2 SEM micrographs of shaddock peel (a), and composites after infiltration for 1 time (b), 2 times (c) and 3 times (d). (e) WGR of shaddock peel after infiltration. (f) Comparison of WGR of infiltrated shaddock peel with other natural materials.

3.2 Effect of heating program on the microstructures of composites

Fig. 3a shows the TG/DTG curves of PCS/shaddock peel composites. The cellulose, hemicellulose and lignin in the shaddock peel and polycarbosilane were decomposed gradually during the pyrolysis from 200 to 800°C. The released gas (i.e. H_2O, CH_4) could cause pores and cracks in SiC matrix (Fig. 3a), so properly controlling the heating program is vital to reduce the pores and cracks. As shown in Fig. 3a, the weight loss of 14.2% at 200 ~ 400 °C was mainly caused by the decomposition of cellulose and hemicellulose from the shaddock peel. The weight loss of 4.6% at 400 ~ 600 °C was mainly caused by the decomposition of lignin and PCS. The weight loss of 8.9% at 600 ~ 800 °C was mainly caused by the decomposition of PCS [34, 35]. In order to complete the conversion of PCS to SiC, PCS was generally pyrolyzed, accompanied by the release of a large number of small molecule gases (i.e. H_2, CH_4, etc.) at 520 ~ 800 ℃ [36]. The weight loss of PCS/shaddock peel composites tends to be constant at 800 ~ 1000°C. Based on the TG/DTG curve of PCS/shaddock peel composites, the heating program was optimized to shorten the processing time and reduce microcracks (Fig. 3c). A heating rate of 5 ℃/min was used in the temperature range from 25 ℃ to 200 ℃. A slow heating rate of 1 ℃/min was used in the temperature ranges of both 200 ~ 400 ℃ and 600 ~ 800 ℃ to release the gas (i.e. H_2, CH_4, H_2O, etc.) from the sample body very slowly. A heating rate of 2 ℃/min was used in the temperature range from 400 ℃ to 600 ℃ to continue releasing the gas slowly. In the range of 800 ℃ to the sintering temperature (1200 ~ 1600 ℃), the heating rate can be increased to 5 ℃/min to shorten the processing time, and the duration time of sintering was 120 mins. The inorganic transformation of PCS was complete at 800 ~ 1200 ℃, and β-SiC crystallization began to occur [23]. The crystallization degree of SiC was further improved above 1200 ℃ [23], so the sintering temperature was set as 1200 ℃, 1400 ℃ and 1600 ℃. Finally, the samples were cooled down to 50 ℃ with a cooling rate of 2 ℃/min. Slow heating/cooling rates (1 ℃/min and 2 ℃/min) were used to efficiently reduce cracks in the samples by avoiding a rapid release of the gases and the

shrinkage of different phases caused by the rapid cooling (>2 ℃/min). For comparison, the heating program-1 commonly used in existing studies was used to sinter the composites using a heating rate of 5 ℃/min and a cooling rate of 2 ℃/min.

Fig. 3b shows the microstructure of the C-SiC-SiO_2 composites sintered at 1200 ℃ by the heating program-1. Macro-cracks are evident in the composites, owing to a large amount of gas (i.e. CH_4, H_2, etc.) released from the polycarbosilane and shaddock peel during the pyrolysis process. Fig. 3c shows the microstructure of the C-SiC-SiO_2 composites sintered at 1200 ℃ by the optimized heating program-2. Few cracks are observed in the composites, because the slower heating rate allows the gases to be released slower.

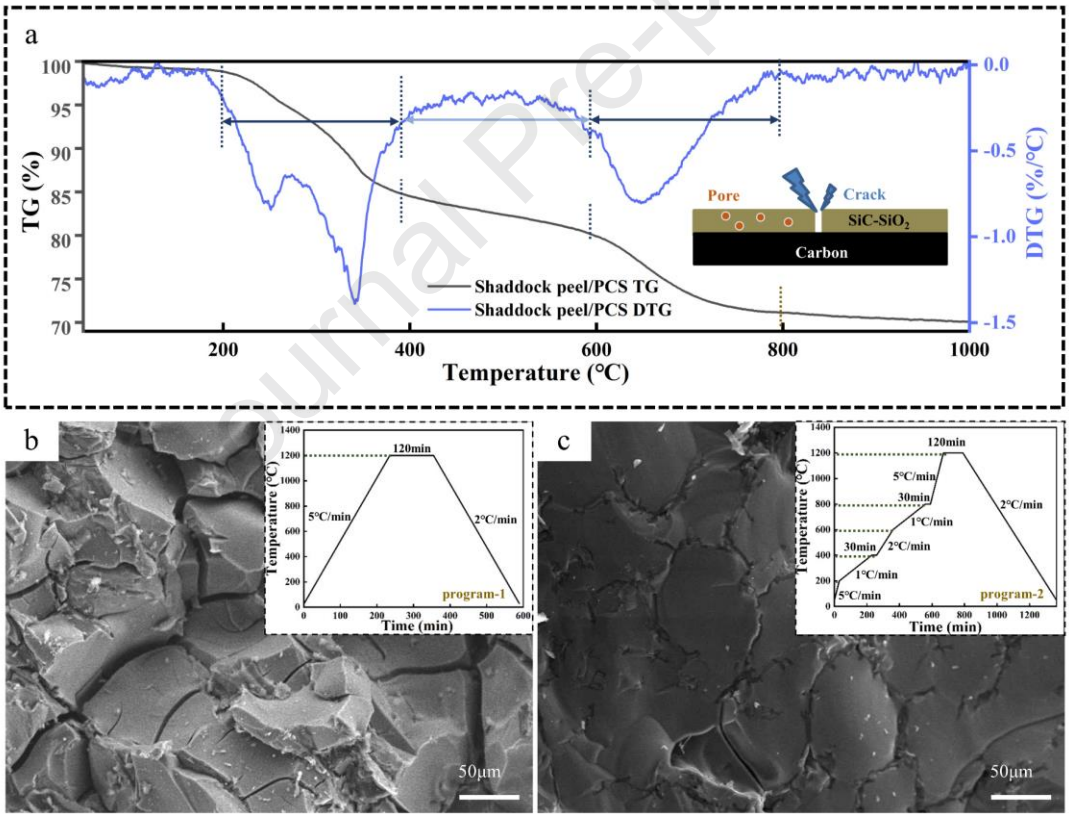

Fig. 3(a) TG and DTG curves of the PCS/shaddock peel composites, (b) SEM micrographs of the C-SiC-SiO_2 composites sintered by the heating program-1 (inset: general heating program-1) and (c) SEM micrographs of the C-SiC-SiO_2 composites sintered by the optimized heating program-2 (inset: optimized heating program-2).

3.3 Effect of sintering temperature on the phase and shrinkage of composites

Fig. 4 shows the XRD patterns of composites sintered at different temperatures (1200 ℃, 1400 ℃ and 1600 ℃) using the optimized heating program-2, where the peaks of SiC, SiO_2 and C are observed in all composites, confirming the successful conversion of PCS in trace oxygen-containing (~ 0.9 vol.%) environment. The strongest peak of SiO_2 is observed at $2\theta = 21.8°$, corresponding to the (101) crystal plane of the SiO_2. The peaks at $2\theta = 36.2°$, $2\theta = 61.2°$, $2\theta = 71.8°$ correspond to the (111), (220), (311) crystal planes of the SiC. The peaks at $2\theta = 27.6°$ correspond to the (111) crystal planes of carbon. All composites show the sharp peaks of SiO_2 and carbon indicating the existence of crystalline SiO_2 and carbon. The composites sintered at 1200 ℃ show the weak peaks of SiC, suggesting it is present in small amount. The composites sintered at 1400 ℃ show three broad peaks of SiC, indicating a poor crystallinity. The composites sintered at 1600 ℃ show sharp peaks of SiC, indicating a good crystallinity.

To sum up, a small amount of SiC can be generated when the composites are sintered at 1200 ℃. The crystallinity of SiC in sintered composites increases with the sintering temperature increasing from 1200 ℃ to 1600 ℃. Due to the existence of oxygen (O_2: ~ 0.9%) in the sintering atmosphere and oxygen atoms from the shaddock peel and PCS, Si-H in polycarbosilane could react with oxygen in the sintering process to generate Si-O-H or Si-O-Si, thus forming SiO_2 phase [36].

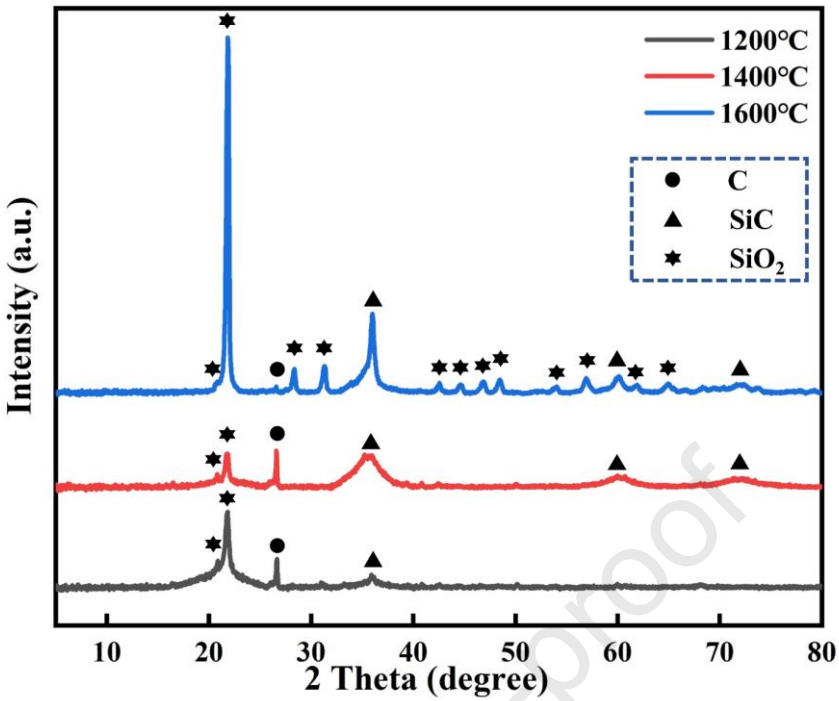

Fig. 4 XRD patterns of the C-SiC-SiO_2 composites sintered at different temperatures (1200 ℃, 1400 ℃ and 1600 ℃).

Fig. 5a shows the drying shrinkage and sintering shrinkage of the sample (18 mm × 18 mm × 8 mm) in different directions (length, width and height), which shows the uniform shrinkage of the samples in the three directions. Fig. 5b shows the summary of shrinkage (Direction: L) of biomorphic composites derived from natural materials. The shrinkage of the shaddock peel-derived composites sintered at 1200 ℃, 1400 ℃ and 1600 ℃ is lower than that of the composites derived from untreated wood (such as birch [22], oak [33] and coir [14]), and it is similar to that of the extracted pine [6, 15] derived composites.

a

Shrinkage of drying	length	2.3% ± 0.8%		
	width	2.5% ± 0.5%		
	height	1.9% ± 0.6%		
Sintering temperature		1200°C	1400°C	1600°C
Shrinkage of sintering	length	19.3% ± 0.8%	19.8% ± 2.2%	22.6% ± 1.2%
	width	19.6% ± 1.4%	20.6% ± 1.7%	23.1% ± 1.15%
	height	16.7% ± 1.4%	17.9% ± 1.9%	18.7% ± 2.5%

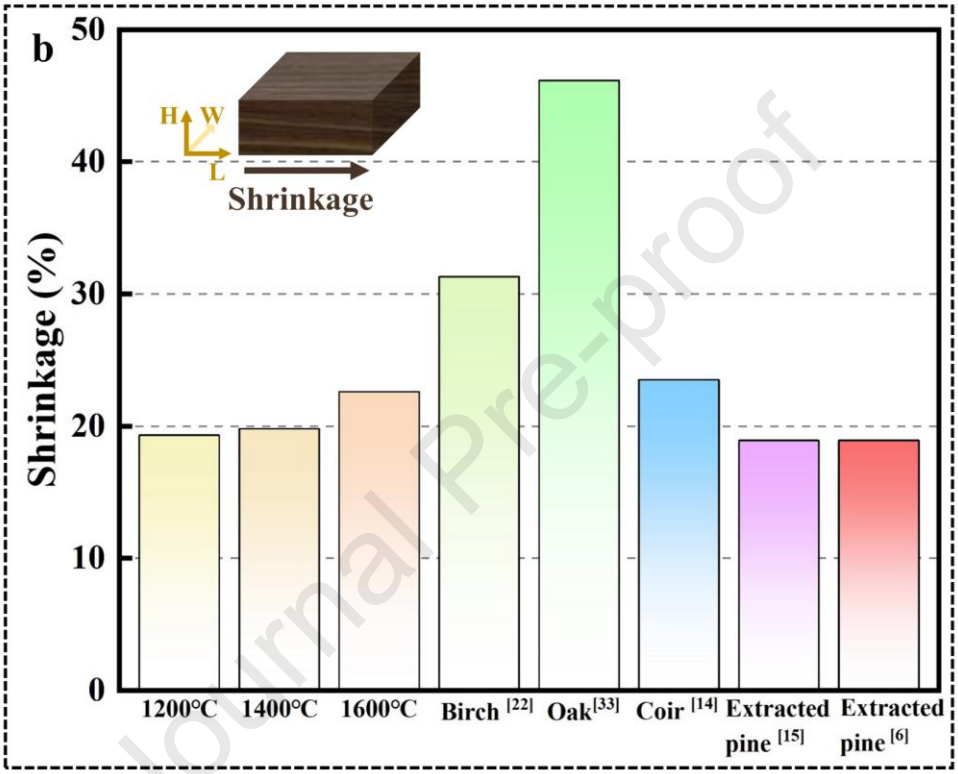

Fig. 5 (a) Drying shrinkage and sintering shrinkage of samples in different directions (length, width and height), (b) Summary of shrinkage (Direction: L) of biomorphic composites derived from natural materials.

3.4 Phase distribution of composites

Fig. 6a-d and i-l show the overall view of the shaddock peel-derived biomorphic C-SiC-SiO_2 composite sintered at 1400 °C, including pores (blue), SiC-SiO_2 (grey) and carbon (red). A uniform distribution of SiC-SiO_2 and pores is observed in the composites, indicating that PCS was efficiently and evenly infiltrated into the shaddock peel (supplementary Fig. S2). Fig. 6e-h show the X-ray computed tomography (CT) of

a virtual slice (located at yellow square in Fig. 6a) in the composites showing pores (blue), SiC-SiO_2 (yellow) and carbon (red). While circular holes derived from shaddock peel and few cracks are observed in the slice (Fig. 6f), the SiC-SiO_2 phases were evenly distributed on the shaddock peel-derived carbon (Fig. 6g) and the template was retained and closely bonded with SiC-SiO_2 (Fig. 6h). Fig. 6m shows the distance from the top surface for each slice versus the volume fraction of pore, carbon and SiC-SiO_2 phase in the composite. The distributions of pores, carbon and SiC-SiO_2 were determined from the X-ray computed tomography (CT) virtual slices and the volume fraction of each phase was calculated from each virtual slice. The volume fraction of pore, carbon and SiC-SiO_2 exhibit only slight fluctuations with the increase of the distance (the distance was calculated along the direction of blue arrow (f) in Fig. 6i, 2000 ~ 20000 μm) from the top surface, indicating a uniform distribution of pores, carbon and SiC-SiO_2 phase in the whole composite. Fig. 6m exhibits the highest volume fraction (70% ± 5%) of the SiC-SiO_2 phase in each CT slice, and relatively lower volume fraction of carbon (volume fraction: 20% ± 5%) and pores (volume fraction: 10% ± 5%) in each CT slice, further indicating the high efficiency of infiltration of PCS into shaddock peel.

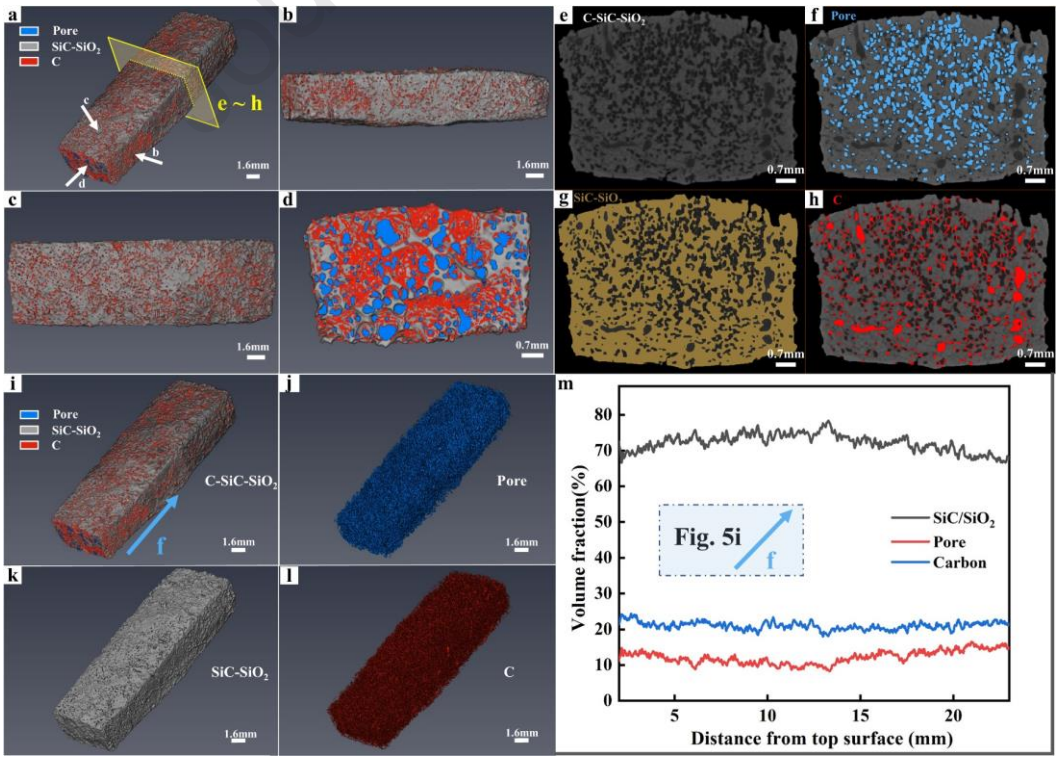

Fig. 6 X-ray computed-tomography of the shaddock peel-derived biomorphic C-SiC-SiO_2 composite sintered at 1400 ℃. (a-d, i-l) Overall view of composite showing pores (blue), SiC-SiO_2 (grey) and carbon (red). (e-h) X-ray computed tomography (CT) of a virtual slice (located at yellow square in Fig. 6a) in composite showing pores (blue), SiC-SiO_2 (yellow) and carbon (red). (m) Distance (along the direction of blue arrow (f) in Fig. 6i) from top surface versus volume fraction of pore, carbon and SiC-SiO_2 phase in the composite.

3.5 Mechanical properties of the composites

The compressive strength and bending strength of all composites sintered at 1200 ℃, 1400 ℃ and 1600 ℃ were evaluated in details. Fig. 7a shows the force-displacement curves in a compression test of the sintered composites at 1200 ℃, 1400 ℃ and 1600 ℃. Fig. 7b shows the force-displacement curves in a bending test of sintered composites at 1200 ℃, 1400 ℃ and 1600 ℃. Supplementary Fig. S3 shows the surface morphology of the C-SiC-SiO_2 composites (sintered at 1200 ℃) after the bending test. All composites sintered at 1200 ℃, 1400 ℃ and 1600 ℃ exhibit the typical zigzag curve as shown in Fig. 7a and b, because the composites are porous and brittle ceramics, in good agreement with Fig. 8a, d and g. Fig. 7c shows the maximum compressive strength, bending strength and specific strength of the composites sintered at 1200 ℃, 1400 ℃ and 1600 ℃. The composites sintered at 1600 ℃ exhibit the highest compressive strength of ~ 14.0 MPa, owing to the highest crystallinity of SiC formed in the composites (as shown in Fig. 4). The composites sintered at 1400 ℃ exhibit the lowest compressive strength of ~ 3.5 MPa, owing to the poor crystallinity of SiC formed in the composites (as shown in Fig. 4). The composites sintered at 1200 ℃ exhibit a higher compressive strength of ~ 11.6 MPa than the composites sintered at 1400 ℃, owing to the well-bonded interface (as shown in Fig. 8a b c) between C and SiC/SiO_2.

The composites sintered at 1200 ℃ exhibit the highest bending strength of ~ 27.4 MPa, owing to the well-bonded interface between C and SiC/SiO_2 (as shown in Fig. 8b) and the uniform shrinkage in length, width and height (as shown in Fig. 5a), while the

composites sintered at 1400 ℃ exhibit a decreased bending strength of ~ 19.5 MPa, owing to the partially split interface between C and SiC/SiO_2 (as shown in Fig. 8e). The composites sintered at 1600 ℃ exhibit the lowest bending strength of ~ 7.4 MPa, owing to the gap between C and SiC/SiO_2 (as shown in Fig. 8h).

Fig. 7c shows the composites sintered at 1200 ℃ exhibit the highest specific strength of 0.8×10^7 N·m/kg, while the composites sintered at 1400 ℃ exhibit the lowest specific strength of 0.3×10^7 N·m/kg. The composites sintered at 1600 ℃ exhibit a higher specific strength of 1.5×10^7 N·m/kg than the composites sintered at 1400 ℃.

Fig. 7d shows the comparison of different properties of the C-SiC-SiO_2 composites derived from natural materials, including bending strength, compressive strength and density. The biomorphic C-SiC-SiO_2 composites derived from shaddock peel have similar compressive strength (~ 14.0 MPa) compared to biomorphic SiC derived from pine (12 ~ 25 MPa), iroko tree (16 ~ 22 MPa) and red oak (26 ~ 84 MPa) [28]. The biomorphic C-SiC-SiO_2 composites derived from shaddock peel have similar bending strength (~ 27 MPa) to biomorphic SiC derived from pine (16 ~ 42 MPa) [24, 29]. The axial bending strength (70 MPa) of the sipo-derived biomorphic SiC decreased by 4.1% compared with that of sipo charcoal (~ 73 MPa) [13], while the bending strength of the C-SiC-SiO_2 composites significantly increased by 20 fold, compared with the original shaddock peel.

The density (~ 1.0 g/cm^3) of the shaddock peel-derived C-SiC-SiO_2 composites was lower than those derived from pine (~ 1.4 g/cm^3), iroko tree (~ 1.7 g/cm^3) and red oak (~ 1.8 g/cm^3) [28] The specific strength of the composites was calculated by dividing the compressive strength by density. The shaddock peel-derived C-SiC-SiO_2 composites exhibit the much higher specific strength of 1.5×10^7 N·m/kg than the biomorphic SiC derived from ayous (0.9×10^7 N·m/kg) and iroko tree (1.3×10^7 N·m/kg) [28].

Fig. 7e shows the diagram of bending test and compression test of composites sintered at 1200 ~ 1600℃, which is based on the interface bonding in Fig. 8. The

influence of interface bonding on the bending strength of the composites is greater than that of the crystallinity of the sample on the bending strength, and the influence of the crystallinity of the sample on the compression strength is greater than that of the interface bonding of the composites on the compression strength, owing to the different stress of compression test and bending test. Some small blocks with good crystallinity have supporting effect in the compression test. The crack in the bending test, usually extends at the poor interface bonding.

To sum up, the shaddock peel-derived biomorphic C-SiC-SiO_2 composites sintered at 1600 ℃ have the highest compressive strength of ~ 14.0 MPa and highest specific strength of ~ 1.5×10^7 N·m/kg, owing to the good crystallinity of SiC. The bending strength of the shaddock peel-derived C-SiC-SiO_2 composites decreased from ~ 27.4 MPa to ~ 7.4 MPa, with the sintering temperature increasing from 1200 ℃ to 1600 ℃. The shaddock peel-derived composites sintered at 1200 ℃ have the highest bending strength of ~ 27.4 MPa, owing to the well-bonded interface between C and SiC/SiO_2 and the uniform shrinkage in length, width and height.

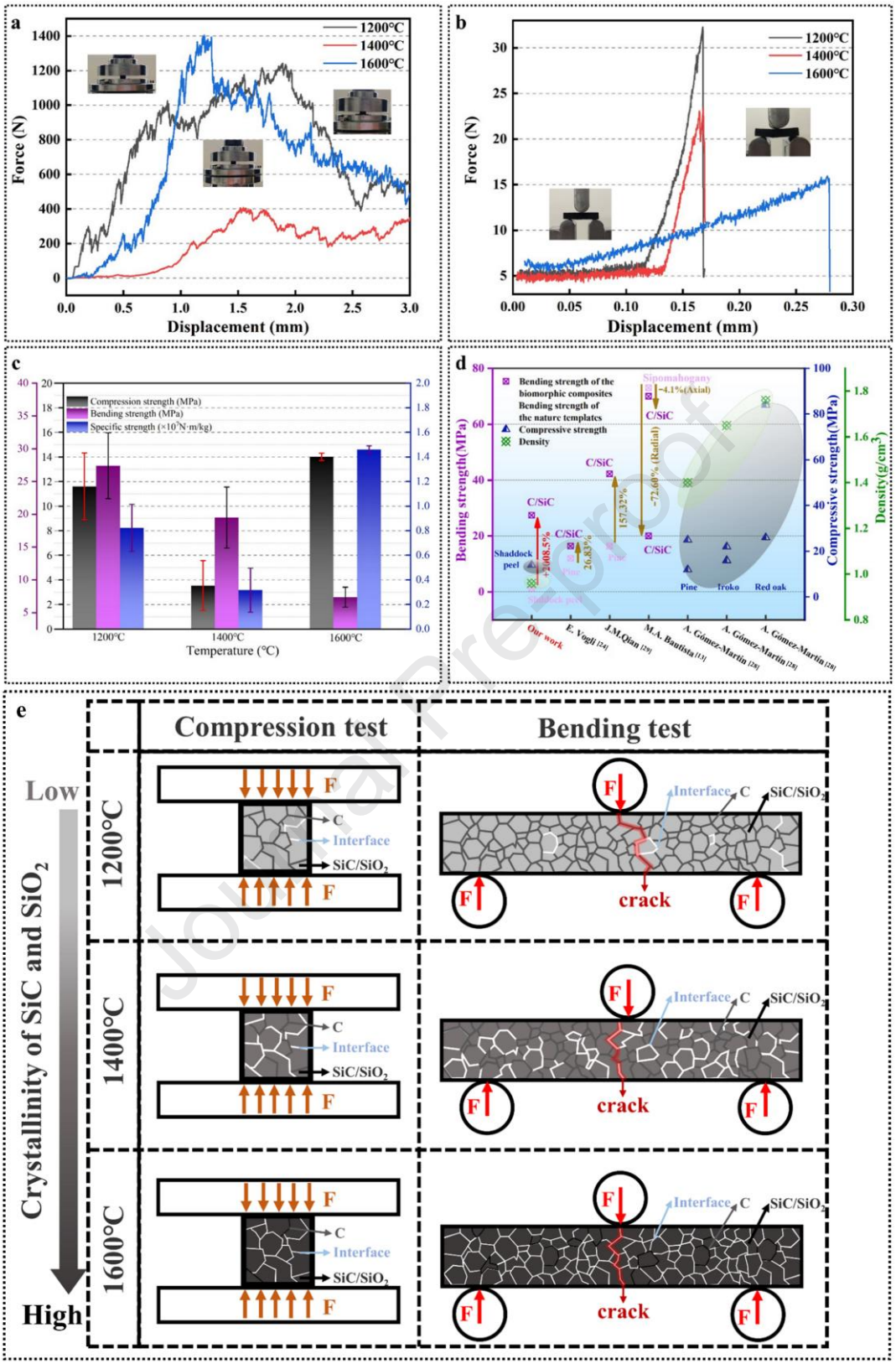

Fig. 7 (a) Force-displacement curves of C-SiC-SiO_2 composites sintered at 1200 ℃, 1400 ℃ and 1600 ℃ in compression tests, (b) Force-displacement curves of C-SiC-SiO_2 composites sintered at

1200 ℃, 1400 ℃ and 1600 ℃ in bending tests, (c) Bar chart of bending strength, compressive strength and specific strength of shaddock peel-derived biomorphic C-SiC-SiO_2 composites sintered at 1200 ~ 1600 ℃ and (d) Summary of properties (i.e. density, compressive strength and bending strength) of biomorphic composites derived from natural materials, (e) the diagram of bending test and compression test of composites sintered at 1200 ~ 1600 ℃.

Fig. 8a-c, d-f and g-i are the cross-sections of the shaddock peel-derived biomorphic C-SiC-SiO_2 composites sintered at 1200 ℃, 1400 ℃ and 1600 ℃, respectively, after bending strength test. The unique three-dimensional interconnected structure of the C-SiC-SiO_2 composites was retained (as shown in the yellow dotted circles in Fig. 8a and supplementary Fig. S4), owing to the PCS evenly distributed on the shaddock peel. The dark part in Fig. 8f is carbon formed by the pyrolysis of shaddock peel, in good agreement with the EDS-mapping in inset. The C-SiC-SiO_2 composites sintered at 1200 ℃ have a closely bonded interface between C and SiC/SiO_2 (as shown in Fig. 8b and c) and the uniform shrinkage in length, width and height (as shown in Fig. 5a), leading to the outstanding bending strength of ~ 27.4 MPa (Fig. 7c). The C-SiC-SiO_2 composites sintered at 1400 ℃ have a partially separated interface between C and SiC/SiO_2 (as shown in Fig. 8e and f), leading to the decreased bending strength of ~ 19.5 MPa (Fig. 7c). The C-SiC-SiO_2 composites sintered at 1600 ℃ have a gap between C and SiC/SiO_2 (as shown in Fig. 8h and i), leading to the obviously decreased bending strength of ~ 7.4 MPa (Fig. 7c).

Compared with other composites, the composites sintered at 1600 ℃ show higher compressive strength (14.0 MPa) but lower bending strength (7.4 MPa), probably resulting from the calcium (as shown in Fig. 9e, spot.3: Ca: 0.65%) diffusion into SiC/SiO_2 matrix to form calcium and silicon solid solution at high temperature (≥1200 ℃). However, the calcium content in shaddock peel is low, and only a small amount of calcium diffused into SiC matrix, which can only locally strengthen the SiC/SiO_2 matrix.

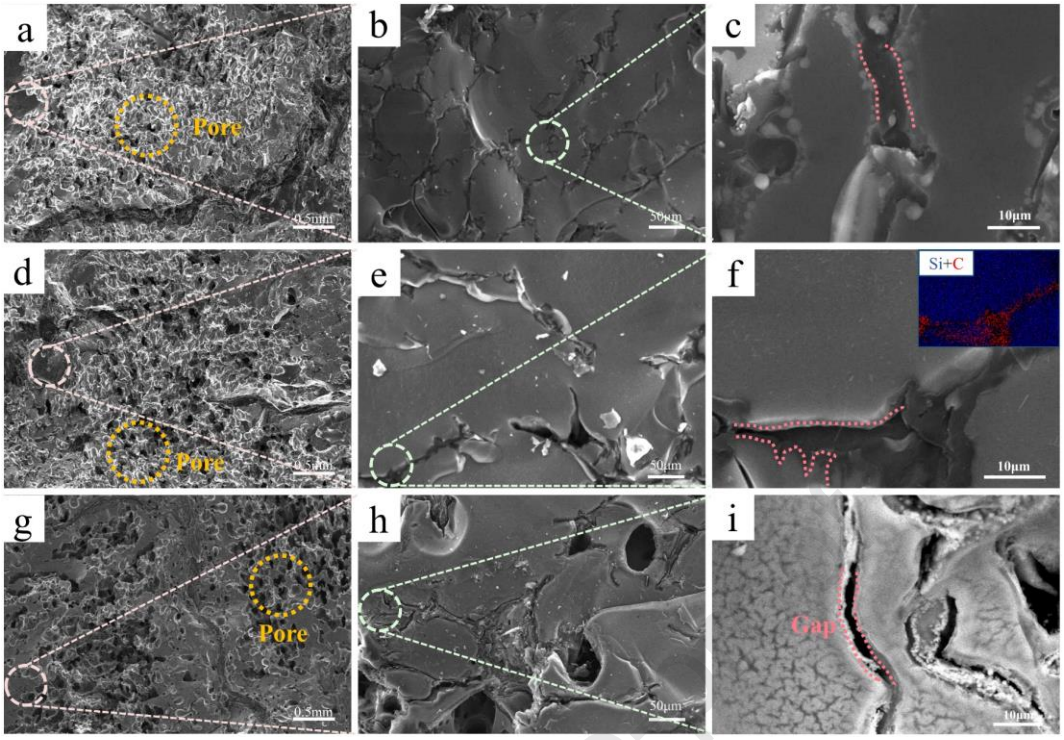

Fig. 8 The cross-sections of the shaddock peel-derived biomorphic C-SiC-SiO_2 composites sintered at 1200 ℃ (a-c) 1400 ℃ (d-f) and 1600 ℃ (g-i). The inset in (f) is the EDS-mapping of the composites corresponding to (f).

3.6 High-temperature oxidation behavior of the composites

Fig. 9a shows the surface morphology of the C-SiC-SiO_2 composites before and after 45 mins oxidation at 500 ~ 1400 ℃. Some white filaments can be observed on the surface of all composites after oxidation at 500 ~ 1400 ℃. The white filaments become more obvious with the oxidation temperature increasing from 500 to 1400 ℃, owing to the oxidation of carbonized shaddock peel. The C-SiC-SiO_2 composites sintered at 1600 ℃ appear partially white at room temperature because those have been oxidized during the sintering process. Fig. 9b is the weight loss (It is calculated by dividing the lost weight of the sample by the sample volume) curve of the C-SiC-SiO_2 composites after oxidation at 500 ~ 1400 ℃. All C-SiC-SiO_2 composites sintered at 1200 ℃, 1400 ℃ and 1600 ℃ exhibit a relatively low weight loss (<0.11 g/cm^3) after oxidation at 1400 ℃, indicating good thermal oxidation resistance (500-1400 ℃) [37-40]. The C-

$SiC-SiO_2$ composites sintered at 1200 ℃ show the highest weight loss of 0.11 g/cm^3, after oxidation at 500 ~ 1400 ℃. The weight loss of the oxidized $C-SiC-SiO_2$ composites sintered at 1600 ℃ is the lowest with ~ 0.05 g/cm^3. The weight changes of the oxidized $C-SiC-SiO_2$ composites were mainly caused by the oxidation of carbonized shaddock peel and the formation of SiO_2. Fig. 9c shows the density of the $C-SiO-SiO_2$ composites before and after oxidation at 500 ~ 1400 ℃. The density of the composites increased slightly after oxidation above 800℃ (the green dotted box), owing to the increase of Si-O-C and SiO_2. Fig. 9d shows the SEM of the $C-SiO-SiO_2$ composite sintered at 1200 ℃ before (left) and after (right) oxidation at 1400 ℃, Si-O-C and SiO_2 coatings were observed on the oxidized surface of the composite. Fig. 9e are the compressive strength and XRD of composites sintered at 1200 ℃ before and after oxidation at 1400 ℃, respectively. The compressive strength (21.5 MPa) of the $C-SiC-SiO_2$ composites after oxidation at 1400 ℃ was increased by 85.4%, compared with the unoxidized $C-SiC-SiO_2$ composites (11.6 MPa). As shown in Fig. 9f, the characteristic peak of SiC after oxidation is sharper than that before oxidation, indicating that the crystallinity of SiC increases during the oxidation process. Fig. 9g is the SEM micrographs and EDS of the composites after oxidation at 1400 ℃. The Si-O-C and SiO_2 coating (supplementary Fig. S5) (spot.1: Si: 26.65%, O: 64.8%, C: 8.55%; spot.2: Si: 27.57%, O: 65.53%, C: 6.84%) can be clearly observed on the SiC/SiO_2 surface (spot.4: Si: 27.16%, O: 60.70%, C: 12.13%) of the composites, indicating the oxygen diffusing into the matrix to form SiO_2 during thermal oxidation. Fig. 9g shows the mechanism of strengthening during thermal oxidation process. Two strengthening mechanisms were proposed to explain the increased compressive strength of the composites after oxidation at 1400 ℃, as below: 1. The glassy Si-O-C phase generated at 1400 ℃ can viscously flow to fill the micro-cracks in the SiC/SiO_2 matrix, as shown in Fig. 9h. 2. The oxygen molecules can diffuse into the ceramic matrix, and the formed SiO_2 might grow along the interface to fill the microcracks [41, 42], as shown in Fig. 9h.

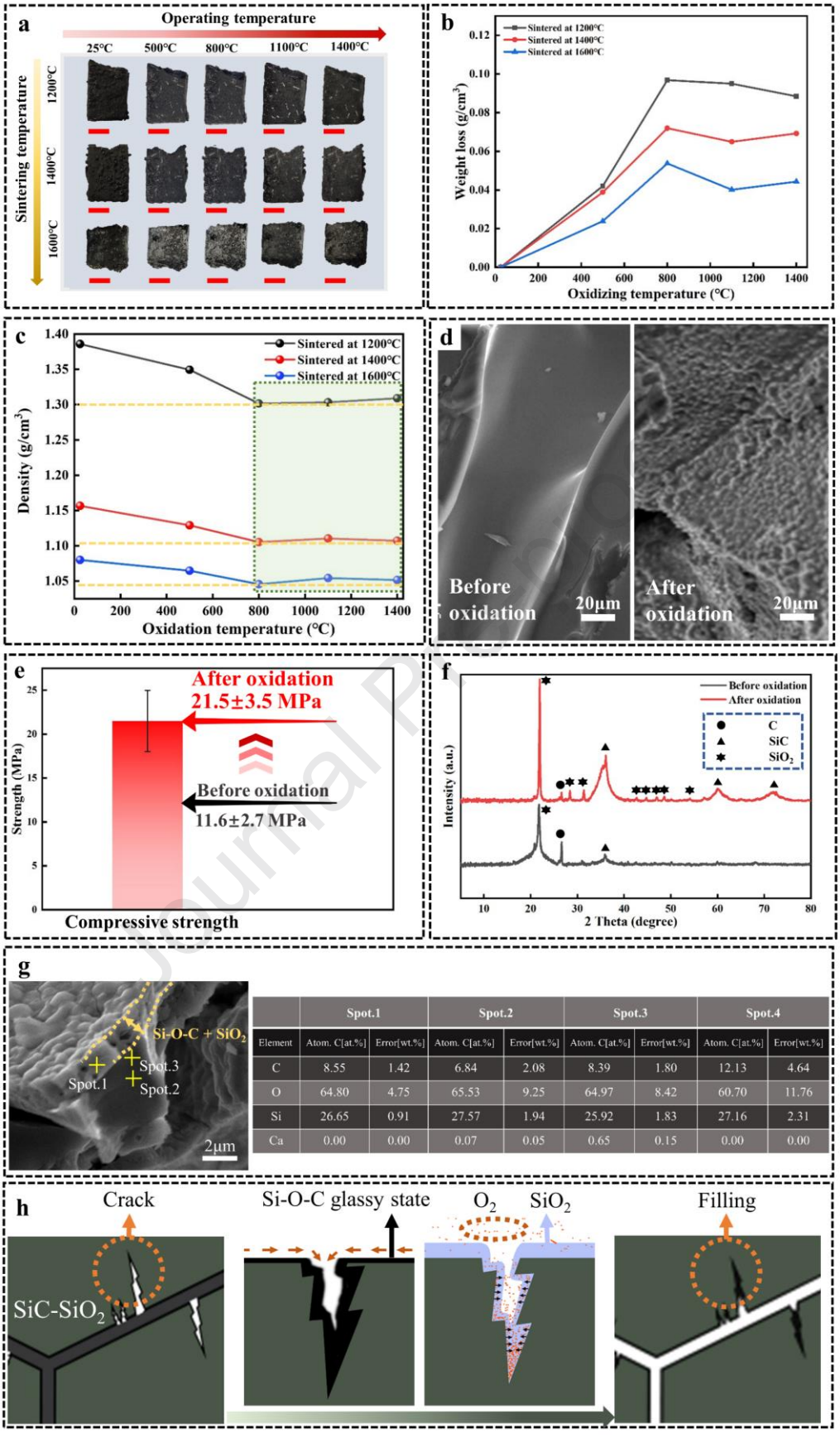

	Spot.1		Spot.2		Spot.3		Spot.4	
Element	Atom. C[at.%]	Error[wt.%]	Atom. C[at.%]	Error[wt.%]	Atom. C[at.%]	Error[wt.%]	Atom. C[at.%]	Error[wt.%]
C	8.55	1.42	6.84	2.08	8.39	1.80	12.13	4.64
O	64.80	4.75	65.53	9.25	64.97	8.42	60.70	11.76
Si	26.65	0.91	27.57	1.94	25.92	1.83	27.16	2.31
Ca	0.00	0.00	0.07	0.05	0.65	0.15	0.00	0.00

Fig. 9 (a) the surface morphology of the C-SiC-SiO_2 composites before and after oxidation at 500 ~ 1400 ℃ (b) the weight loss curves of the composites after oxidation at 500 ~ 1400 ℃ (c) density of the C-SiO-SiO_2 composites before and after oxidation at 500 ~ 1400 ℃ (d) SEM of the C-SiO-SiO_2 composite sintered at 1200 ℃ before (left) and after (right) oxidation at 1400 ℃ (e) the compressive strength of the C-SiO-SiO_2 composites sintered at 1200 ℃ before and after oxidation at 1400 ℃ (f) XRD patterns of the C-SiO-SiO_2 composites sintered at 1200 ℃ before and after oxidation at 1400 ℃ (g) SEM and EDS of the oxidized composites and (h) the proposed strengthening mechanisms of the C-SiC-SiO_2 composites during the thermal oxidation at 1400 ℃.

4. Conclusions

The shaddock peel-derived bulk C-SiC-SiO_2 composites were obtained by introducing PCS into a shaddock peel, using polymer precursor infiltration (PPI). The unique three-dimensional interconnected structure of the shaddock peel is beneficial to easily infiltrate PCS, leading to a weight gain rate of up to 541%. The heating program was optimized according to TGA to successfully prepare the bulk C-SiC-SiO_2 composites with few cracks, low density (0.96 g/cm^3) and uniform microstructure (uniformly distributed C/SiC/SiO_2 and pores). The mechanical properties of the composites were significantly affected by the C/SiC/SiO_2 interfacial bonding and SiC crystallinity. The composites sintered at 1600 ℃ have the highest compressive strength of ~ 14.0 MPa and highest specific strength of ~ 1.5 × 10^7 N·m/kg, owing to the good crystallinity of SiC. The bending strength of the C-SiC-SiO_2 composites decreased from ~ 27.4 MPa to ~ 7.4 MPa, with the sintering temperature increasing from 1200 ℃ to 1600 ℃. The composites sintered at 1200 ℃ have the highest bending strength of ~ 27.4 MPa, owing to the well-bonded interface between C and SiC/SiO_2. The thermal oxidation of the composites mainly includes the oxidation of carbon and SiC, and the weight loss of all composites is less than 0.11 g/cm^3, showing outstanding thermal stability. The compressive strength (~ 21.5 MPa) of the composites (sintered at 1200 ℃) after oxidation at 1400 ℃ increased by 85.3%, compared with those (~ 11.6 MPa) before oxidation. The proposed strengthening mechanisms of the composites during the

thermal oxidation at 1400 ℃ were further confirmed by SEM, indicating the micro-cracks in the SiC/SiO_2 matrix might be filled by the formed Si-O-C phase and SiO_2 phase. The shaddock peel-derived $C\text{-}SiC\text{-}SiO_2$ composites are the light material with high strength and excellent high-temperature thermal oxidation resistance. The benefits of using shaddock peel to produce composites with high specific strength, are to both easily make complex-shaped materials and reuse the waste.

Acknowledgement

The authors gratefully acknowledge the support of Natural Science Foundation of Jiangsu province (No. BK20200455), National Natural Science Foundation of China (No. 52002174), Innovation and entrepreneurship program of Jiangsu province, Changkong star program from Nanjing University of Aeronautics and Astronautics, and Postgraduate Research & Practice Innovation Program of NUAA (xcxjh20210621). Many thanks to Rong Rong for SEM tests and Zhe Wang for CT tests.

Appendix A. Supplementary data

Supplementary data related to this article can be found at xxx

References

[1] M. Yu, G. j. Zhang, T. Saunders, Wood-derived ultra-high temperature carbides and their composites: A review, Ceramics International, 46 (2020) 5536-5547.

[2] A. Xfw, A. Jxl, B. Wb, Q. A. Yuan, L. A. Fei, A. Yl, B. Fx, A. Gjz, High-entropy carbide ceramics with refined microstructure and enhanced thermal conductivity by the addition of graphite, Journal of the European Ceramic Society, 41 (2021) 4747-4754.

[3] Y. Zeng, D. Wang, X. Xiong, X. Zhang, P. J. Withers, W. Sun, M. Smith, M. Bai, P. Xiao, Ablation-resistant carbide Zr0.8Ti0.2C0.74B0.26 for oxidizing environments up to 3,000 degrees C, Nat Commun, 8 (2017) 15836.

[4] S. Zhang, X. Li, J. Zuo, J. Qin, K. Cheng, Y. Feng, W. Bao, Research progress on active thermal protection for hypersonic vehicles, Progress in Aerospace Sciences, 119 (2020) 100646.

[5] Q. Xu, X. Liu, Q. Luo, Y. Song, H. Wang, M. Chen, Y. Xuan, Y. Li, Y. Ding, Bifunctional biomorphic SiC ceramics embedded molten salts for ultrafast thermal and solar energy storage, Mater Today Energy, 21 (2021) 100764.

[6] J. Locs, L. Berzina-Cimdina, A. Zhurinsh, D. Loca, Optimized vacuum/pressure sol impregnation processing of wood for the synthesis of porous, biomorphic SiC ceramics, Journal of the European Ceramic Society, 29 (2009) 1513-1519.

[7] J. M. Qian, J. P. Wang, Z. H. Jin, Preparation of biomorphic SiC ceramic by carbothermal reduction of oak wood charcoal, Mat Sci Eng a-Struct, 371 (2004) 229-235.

[8] G. J. Qiao, Z. H. Jin, J. M. Qian, Biomorphic SiC ceramics prepared by organic template method, Key Eng Mat, 317-318 (2006) 167-172.

[9] M. J. Lopez-Robledo, A. Gomez-Martin, J. Ramirez-Rico, J. Martinez-Fernandez, Sliding wear resistance of porous biomorphic sic ceramics, Int J Refract Met H, 59 (2016) 26-31.
[10] K. C. Hung, T. L.Wu, J. W. Xu, Preparation of Biomorphic Porous SiC Ceramics from Bamboo by Combining Sol–Gel Impregnation and Carbothermal Reduction, Polymers-Basel, 11 (2019) 1442.
[11] U. Vogt, A. Herzog, T. Graule, R. Klinger, T. Zimmermann, O. Paris, Wood Derived SiC Ceramics with Oriented Porous Structures via Carbothermal Reduction, High Temperature Ceramic Matrix Composites2001, pp. 420-426.
[12] H. Yamane, F. Kawamura, T. Yamada, Low-temperature synthesis of biomorphic cellular SiC ceramics from wood by using a Na flux, J Ceram Soc Jpn, 116 (2008) 163-165.
[13] M. A. Bautista, J. Q. Cancapa, J. M. Fernandez, M. A. Rodríguez, M. Singh, Microstructural and mechanical evaluation of porous biomorphic silicon carbide for high temperature filtering applications, Journal of the European Ceramic Society, 31 (2011) 1325-1332.
[14] A. Maity, D. Kalita, N. Kayal, T. Goswami, O. Chakrabarti, P.G. Rao, Synthesis of biomorphic SiC ceramics from coir fibreboard preform, Ceramics International, 38 (2012) 6873-6881.
[15] A. Zhurinsh, J. Locs, L. Berzina-Cimdina, Investigation of the feasibility of pyrolytic obtaining of porous biomorphic SiC ceramics, J Anal Appl Pyrol, 85 (2009) 544-548.
[16] T. E. Wilkes, M. L. Young, R. E. Sepulveda, D. C. Dunand, K. T. Faber, Composites by aluminum infiltration of porous silicon carbide derived from wood precursors, Scripta Materialia, 55 (2006) 1083-1086.
[17] U. Vogt, A. Herzog, T. Graule, R. Klinger, O. Paris, Wood Derived SiC Ceramics with Oriented Porous Structures via Carbothermal Reduction, Wiley-VCH Verlag GmbH & Co. KGaA2006.
[18] C. Pflitsch, B. Curdts, B. Atakan, Atmospheric Pressure Chemical Vapor Infiltration (CVI) for the Preparation of Biomorphic SiC Ceramics Derived from Paper, J Nanosci Nanotechno, 11 (2011) 8416-8419.
[19] J. T. Zhu, F. L. Kwong, D. H. L. Ng, Synthesis of Biomorphic SiC Ceramic from Bamboo Charcoal, J Nanosci Nanotechno, 9 (2009) 1564-1567.
[20] L. Y. Wang, R. Y. Luo, G. Y. Cui, Z. F. Chen, Effects of pyrolysis temperatures on the oxidation behavior of PIP-processed SiCf/SiC composites, Ceramics International, 46 (2020) 17846-17856.
[21] Y. Zeng, D. Wang, X. Xiong, X. Zhang, P. J. Withers, W. Sun, M. Smith, M. Bai, P. Xiao, Ablation-resistant carbide Zr(0.8)Ti(0.2)C(0.74)B(0.26) for oxidizing environments up to 3,000 °C, Nat Commun, 8 (2017) 15836.
[22] M. Adam, M. Oschatz, W. Nickel, S. Kaskel, Preparation of hierarchical porous biomorphic carbide-derived carbon by polycarbosilane impregnation of wood, Microporous & Mesoporous Materials, 210 (2015) 26-31.
[23] M. Birot, J. P. Pillot, J. Dunogues, Comprehensive Chemistry of Polycarbosilanes, Polysilazanes, and Polycarbosilazanes as Precursors of Ceramics, Chemical Reviews, 95 (1995) 1443-1477.
[24] E. Vogli, H. Sieber, P. Greil, Biomorphic SiC-ceramic prepared by Si-vapor phase infiltration of wood, Journal of the European Ceramic Society, 22 (2002) 2663-2668.
[25] H. Kuisch, J. Van den Bulcke, J. M Baetens, J. Van Acker, Cracking the code: real-time monitoring of wood drying and the occurrence of cracks, Wood Sci Technol, 54 (2020) 1029-1049.
[26] Z. Zhang, L. Cheng, J. Tan, W. Yang, Efficient fabrication of carbon/silicon carbide composite for electromagnetic interference shielding applications, Ceramics International, 47 (2021) 23942-23949.
[27] A. Montón, F. Maury, G. Chevallier, C. Estournès, M. Ferrato, D. Grossin, Densification of surface-modified silicon carbide powder by spark-plasma-sintering, Journal of the European Ceramic Society,

41 (2021) 7543-7551.
[28] A. Gomez-Martin, M. P. Orihuela, J. A. Becerra, J. Martinez-Fernandez, J. Ramirez-Rico, Permeability and mechanical integrity of porous biomorphic SiC ceramics for application as hot-gas filters, Materials & Design, 107 (2016) 450-460.
[29] J. M. Qian, Z. H. Jin, Preparation and characterization of porous, biomorphic SiC ceramic with hybrid pore structure, Journal of the European Ceramic Society, 26 (2006) 1311-1316.
[30] J. M. Qian, J. P. Wang, G. J. Qiao , Z. H. Jin, Preparation of porous SiC ceramic with a woodlike microstructure by sol-gel and carbothermal reduction processing, Journal of the European Ceramic Society, 24 (2004) 3251-3259.
[31] L. Zhou, Y. Cheng, W. Zhang, W. Zhang, W. Liu, Y. Li, M. Wang, Improving the ceramic yield of polycarbosilane by radiation cross-linking in the presence of multifunctional monomers, Int J Appl Ceram Tec, 15 (2018) 1510-1517.
[32] C. R. Rambo, J. Cao, O. Rusina, H. Sieber, Manufacturing of biomorphic (Si,Ti,Zr)-carbide ceramics by sol–gel processing, Carbon, 43 (2005) 1174-1183.
[33] J. Li, S. Yu, M. Ge, X. Wei, Y. Qian, Y. zhou, W. Zhang, Fabrication and characterization of biomorphic cellular C/SiC–ZrC composite ceramics from wood, Ceramics International, 41 (2015) 7853-7859.
[34] L. Cao, J. Chen, C. Liu, X. Liang, Q. Huang, Ceramization mechanism of polycarbosilane treated with high temperature, Zhongnan Daxue Xuebao (Ziran Kexue Ban)/Journal of Central South University (Science and Technology), 45 (2014) 52-57.
[35] L. Liu, L. Cao, H. Niu, J. Wang, Zinc Metal–Organic Framework Growing on the Surface of Fruit Peels and Its Photocatalytic Activity, Acs Omega, 6 (2021) 10187-10195.
[36] Y. J. Joo, K. E. Khishigbayar, K. Y. Cho, C. J. Kim, Reduced Pressure Curing on Polycarbosilane Precursor for Synthesis of Silicon Carbide Fiber, Fibers and Polymers, 19 (2018) 1806-1812.
[37] X. G. Luan, X. Xu, L. Wang, Y. Zou, R. Riedel, L. Cheng, Long-term oxidation behavior of C/SiC-SiBCN composites in wet oxygen environment, Journal of the European Ceramic Society, 41 (2021) 1132-1141.
[38] J. Dai, J. Sha, Y. Zu, Z. Zhang, X. Zou, M. Lei, Microstructural tailoring and its influence on oxidation resistance of carbon fiber-reinforced C-SiC matrix composites, Ceramics International, 45 (2019) 2044-2052.
[39] T. Li, Y. Zhang, Y. Fu, J. Sun, J. Zhang, High strength retention and improved oxidation resistance of C/C composites by utilizing a layered SiC ceramic coating, Ceramics International, 47 (2021) 13500-13509.
[40] D. Zhang, H. Yu, A. Wang, Q. Wang, L. Ren, P. Hu, D. Sun, Achieving the synergy of superior damage tolerance and oxidation resistance of 2D Cf/ZrB2-SiC composites via fiber heat treatment, Applied Surface Science, 556 (2021) 149807.
[41] S. Chen, Y. Zeng, X. Xiong, H. Lun, Z. Ye, T. Jiang, L. Yang, J. Zhang, L. Liu, G. Wang, L. Jing, X. Xie, C. Yan, Static and dynamic oxidation behaviour of silicon carbide at high temperature, Journal of the European Ceramic Society, 41 (2021) 5445-5456.
[42] Y. Li, Y. Ma, Y. Li, S. Li, Processing and microstructure-permeation properties of silica bonded silicon carbide ceramic membrane, Journal of the European Ceramic Society, 41 (2021) 7525-7532.

Declaration of interests

☒ The authors declare that they have no known competing financial interests or personal relationships that could have appeared to influence the work reported in this paper.

☐The authors declare the following financial interests/personal relationships which may be considered as potential competing interests:

2022-06-13

Enhanced strength and thermal oxidation resistance of shaddock peel-polycarbosilane-derived þÿC SiC SiO2 composites

Li, Guo-Qing

Elsevier

Li G-Q, Yu M, Lin G-W, et al., (2022) Enhanced strength and thermal oxidation resistance of þÿshaddock peel-polycarbosilane-derived C SiC SiO2 composites. Ceramics
Volume 48, Issue 19, Part A, October 2022, pp. 27516-27526
https://doi.org/10.1016/j.ceramint.2022.06.045